The Influence of Cobalt, Tantalum, and Tungsten on the Microstructure of Single Crystal Nickel-Base Superalloys

M. V. NATHAL and L. J. EBERT

The influence of composition on the microstructure of single crystal nickel-base superalloys was investigated. Co was replaced by Ni, and Ta was replaced by either Ni or W, according to a matrix of compositions based on MAR-M247.* Substitution of Ni for Co caused an increase in γ' solvus temperature, an increase in γ-γ' lattice mismatch, and the precipitation of W-rich phases in the alloys with high refractory metal levels. Substitution of Ni for Ta caused large decreases in γ' solvus temperature, γ' volume fraction, and γ-γ' lattice mismatch, whereas substitution of W for Ta resulted in smaller decreases in these features. For the alloys with γ' particles that remained coherent, substitution of Ni for Co caused an increase in γ' coarsening rate. The two alloys with the largest magnitude of lattice mismatch possessed γ' particles which lost coherency during unstressed aging and exhibited anomalously low coarsening rates. Creep exposure at 1000 °C resulted in the formation of γ' lamellae oriented perpendicular to the applied stress axis in all alloys.

I. INTRODUCTION

SEVERAL alloying elements in nickel-base superalloys, such as Co and Ta, have been classified as strategic materials as a result of limitations in their supply.[1] Consequently, the effects of these elements on the microstructure and properties of nickel-base superalloys has received renewed attention. Cobalt in particular has been studied extensively, and reviews of early work can be found in references.[1,2,3] These early studies found that additions of 10 to 20 wt pct Co were beneficial for creep-rupture properties in most cases. These property changes were related to the influences of Co on the amount of γ', the amount and type of carbides, stacking fault energy, the formation of grain boundary denuded zones, and the formation of TCP phases.

Recent work on more modern polycrystalline superalloys has confirmed many of the earlier conclusions. In studies of superalloys which had a range of γ' volume fractions, WASPALOY,[4]** UDIMET-700,[5]† and MAR-M247,[2,3] it was found that Co additions generally increased the creep resistance of the alloys but had only minor effects on tensile properties. However, it did appear that Co levels could be reduced to at least one-half of the standard levels in these alloys. Again, these results were related to γ' volume fraction and particle size distributions, carbide type and morphology, and stacking fault energy.

The present investigation extends the previous work to include single crystal superalloys. These alloys do not require the grain boundary strengtheners C, B, Zr, and Hf. The absence of grain boundary elements can change the roles of the other alloying elements. For example, in polycrystalline MAR-M247, most of the Ta is present in the MC carbides; whereas in the single crystal version, C is absent and the Ta is free to partition between the γ and γ' phases. Therefore, the influence of Co and Ta on the microstructure of single crystal MAR-M247 was examined. Tungsten was also studied as a substitute for Ta. The influence of these elements on the tensile and creep strength of these alloys is presented in a companion paper.[6]

**WASPALOY is a trademark of United Technologies Corporation.
†UDIMET is a trademark of Special Metals Corporation.

*MAR-M is a trademark of Martin Marietta Company.

M. V. NATHAL, Research Metallurgist, is with NASA Lewis Research Center, Cleveland OH, 44135. L. J. EBERT, Professor of Metallurgy and Materials Science, is with Case Western Reserve University, Cleveland, OH 44106.

Manuscript submitted November 15, 1984.

II. MATERIALS AND PROCEDURES

Eight single crystal compositions were directionally solidified by the withdrawal process. The chemical analyses of these alloys are given in Table I. Alloy G is the standard MAR-M247 stripped of C, B, Zr, and Hf. Cobalt was replaced by Ni to form Alloy E with 5 pct Co and Alloy B with 0 pct Co where all compositions are in weight percent unless otherwise noted. The role of Ta was investigated by replacing Ta with Ni at each Co level, producing Alloys A, D, and F. Additionally, W was chosen as a substitute for Ta because it is close to Ta in the periodic table, it is known to partition to γ' in some alloys, and it is not considered a strategic element. The W substitution produced Alloys C and H, with 0 and 10 pct Co, respectively.

Two other features of the compositions should also be noted. First, Alloys A, C, D, F, and H possessed W contents which were approximately 1 pct below the intended level. Thus, although Alloys A, D, and F were intended as a series with Ta removed from the baseline level, these alloys had an additional reduction of 1 pct W. Similarly, Alloys C and H were intended as a series with 3 pct W substituted for the baseline 3 pct Ta, but actually only 2 pct W was substituted for the Ta. Thus, in the remainder of this paper, the following notation will be used to designate the alloys:

Alloys B, E, and G will be designated as the 3Ta-10W series.
Alloys A, D, and F will be designated as the 0Ta-9W series.
Alloys C and H will be designated as the 0Ta-12W series.

Finally, it should be noted that Alloy B is also known as NASAIR 100[7] and Alloy E is very close to the composition of Alloy 3 in Reference 7.

Table I. Composition of Single Crystal Alloys (Wt Pct)

	A	B	C	D	E	F	G	H
Ni	74.3	69.7	72.3	69.7	66.4	64.7	61.7	62.5
Co	0	0	0	5.2	5.0	10.1	10.1	10.1
Ta	0	2.82	0	0	2.98	0	2.8	0
W	9.2	10.2	11.8	9.0	9.9	9.0	9.7	11.7
Al	5.2	5.7	5.3	5.2	5.2	5.3	5.2	5.3
Cr	9.2	9.2	8.6	8.8	8.5	8.9	8.5	8.6
Ti	1.4	1.5	1.4	1.4	1.4	1.4	1.4	1.2
Mo	0.7	1.0	0.6	0.7	0.6	0.7	0.6	0.7
C	0.002	0.005	0.005	0.003	0.004	0.004	0.006	0.002
O*	32	20	37	27	33	30	37	50
N*	3	4	3	3	5	3	4	4
B	0.001	0.003	0.005	0.001	0.002	0.001	0.001	0.001
Zr	<0.01	<0.01	<0.01	<0.01	<0.01	<0.01	<0.01	<0.01

Note: * ppm

A standard commercial heat treating schedule was employed for all compositions; it consisted of a solution treatment of 1302 ± 3 °C for four hours followed by forced air quenching, a simulated coating cycle of 982 °C for five hours, and a final age of 871 °C for 20 hours.

Samples for optical and scanning electron microscopy (SEM) were prepared metallographically and etched with a solution of 33 pct nitric acid, 33 pct acetic acid, 33 pct water, and 1 pct hydrofluoric acid. Transmission electron microscopy (TEM) specimens were prepared by twin jet electropolishing with either 10 pct perchloric acid in methanol at −78 °C or 10 pct perchloric acid in acetic acid at room temperature. Phase extractions were performed according to standard procedures.[8] A platinum mesh was used as a cathode, and all extractions were run at room temperature with a current density of 75 to 85 ma/cm^2. The compositions of the γ and γ' phases which were separated by phase extraction were analyzed by inductively coupled plasma atomic emission spectrometry.

X-ray diffraction using copper Kα radiation was employed to measure the lattice mismatch between the γ and γ' phases at room temperature. Single crystal disks with faces parallel to (210) planes were polished and used for the X-ray experiments. Diffractometer scans of the (420) fundamental reflections and of the (210) superlattice reflection were then used to measure the misfit. The γ' lattice parameters were also measured on the extracted γ' residues.

III. RESULTS AND DISCUSSION

A. *Results*

1. *As-cast microstructure*

A dendritic structure was evident in all specimens. The primary dendrite arm spacing varied along the length of a bar from a single casting, reflecting the changes in thermal gradient and growth rate during the solidification process. Typical primary arm spacings were about 200 μm at the bottom of the bar and 550 μm at the top. Because solidification parameters such as mold temperature and withdrawal rate were varied from casting to casting in attempts to improve single crystal yield, the dendrite arm spacings also varied from casting to casting. The interdendritic regions were characterized by coarse γ' structures. In some alloys, large γ' eutectic pools were present, whereas other alloys did not exhibit eutectic pools but did contain areas of coarse γ'. Microprobe scans revealed that the interdendritic regions were high in Ti, Ta, Al, and Ni, and low in Cr, Co, and W.

Differential Thermal Analysis (DTA) was performed on the as-cast samples to establish the influence of composition on the transformation temperatures. These results are summarized in Figure 1. It can be seen that Co level did not strongly influence the liquidus or solidus temperatures, but there were some effects caused by the Ta and W contents. The γ' solvus was strongly influenced by both Co and refractory metal concentrations. The solvus increased by as much as 53 °C as Co level was reduced from 10 to 0 pct, depending on the refractory metal content. Removal of 3 pct Ta and 1 pct W in alloys A, D, and F caused a drop in solvus of 57°, whereas replacement of Ta with 2 pct W resulted in a decrease of 45°. The difference between the solvus and solidus is considered to be the solution treatment "window,"

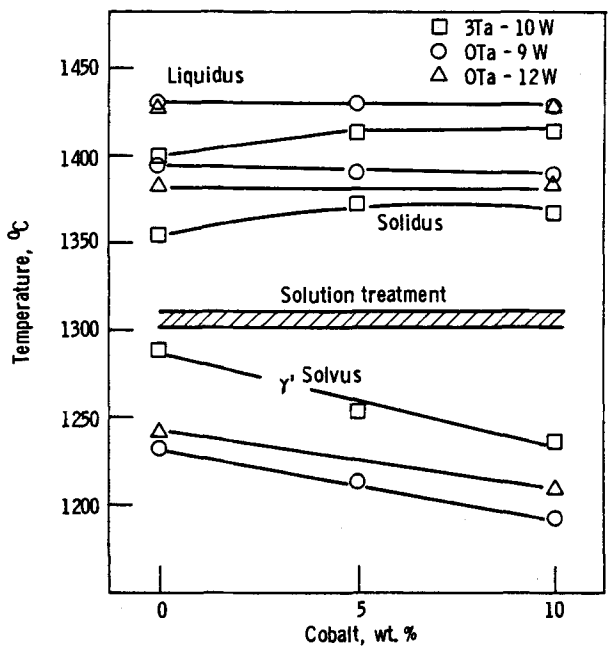

Fig. 1—Results of differential thermal analysis exhibiting the transformation temperatures and heat treatment range for the single crystal alloys.

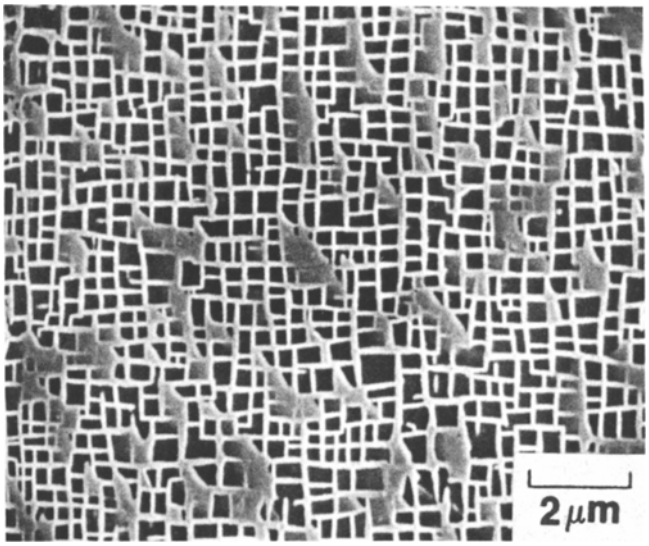

(*a*)

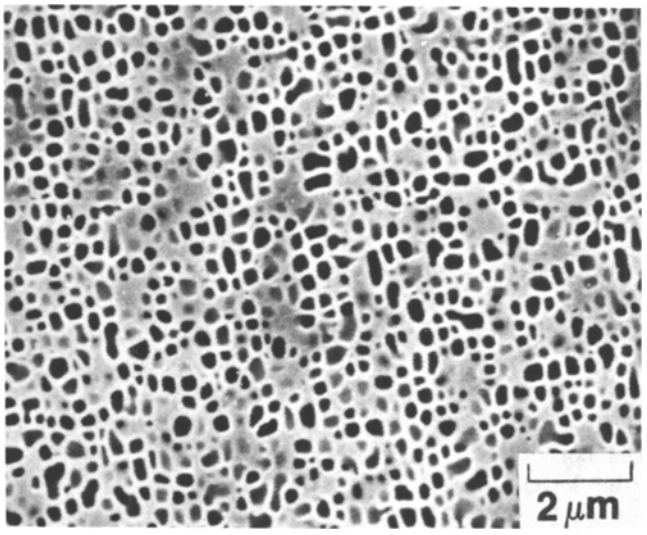

(*b*)

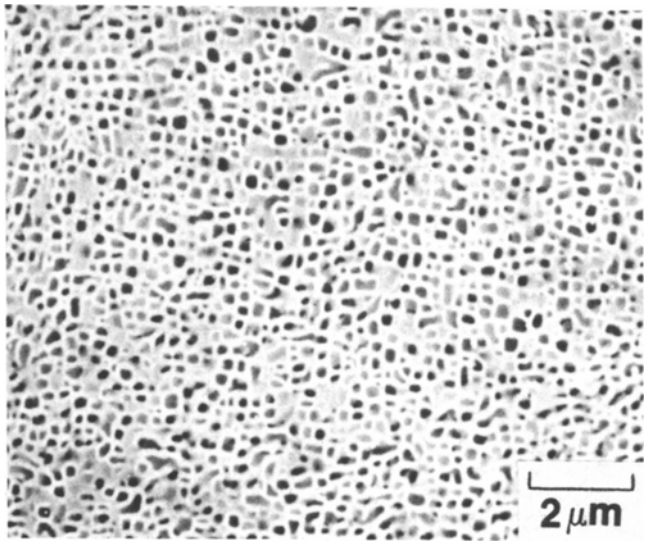

(*c*)

Fig. 2 — Scanning electron micrographs of fully heat treated single crystal alloys. Cubic and spherical γ' morphologies are illustrated. (*a*) Alloy B, (*b*) Alloy A, and (*c*) Alloy G.

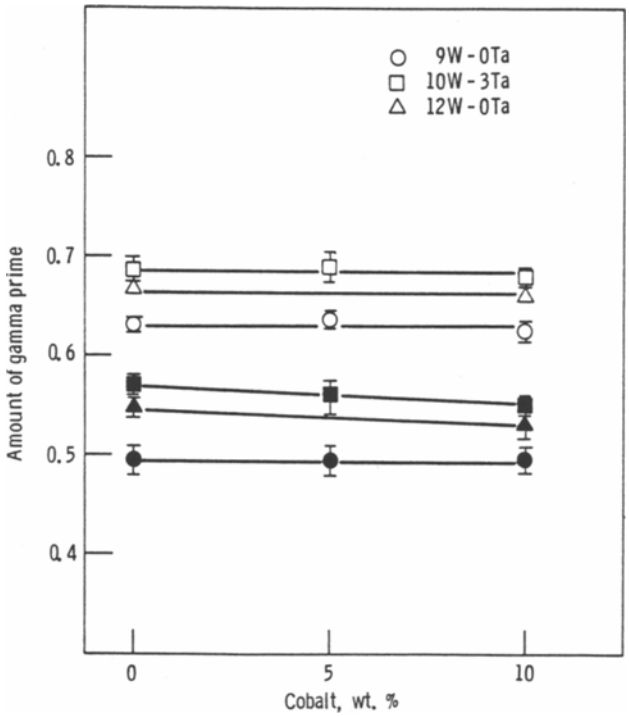

Fig. 3 — The amount of γ' phase in the single crystal alloys. Open symbols correspond to weight fraction as determined by phase extraction experiments on heat treated samples. Closed symbols correspond to volume fraction as determined by quantitative metallography on failed creep-rupture specimens.

and it can be seen that all alloys had an adequate range for complete dissolution of the γ' phase without the danger of incipient melting. These DTA results were confirmed by trial heat treatments in conjunction with optical metallography.

2. *Heat treated microstructure*

The coarse as-cast γ' structures were completely dissolved by the 4-hour solution treatment. In addition, dendritic segregation was reduced to below the sensitivity of the microprobe. However, some residual segregation was still present, because the dendritic pattern was still revealed by etching. In Alloy B, W-rich precipitates were present after the solution treatments. These precipitates decorated the dendrite cores, again indicating that some residual segregation remained after the solution treatment.

The fine distribution of γ' precipitates is illustrated in Figures 2(a) through (c). The γ' particles ranged from a cubical shape, as in Alloy B, to more rounded shapes, as in Alloys A and G. The average γ' particle size of fully heat treated Alloy B was 0.25 μm, as measured by the line intercept technique. The γ' size varied slightly from alloy to alloy. The variations in size were probably caused by a combination of the changes in composition and any variations in quenching rate from the solution treatment. In addition, only slight variations in γ' size existed between the top and bottom of the bars, and across dendritic and interdendritic areas.

The amount of γ' precipitate in each alloy is shown in Figure 3. The weight percent of γ', as measured by phase extraction experiments, was significantly influenced by Ta and W levels, but not by the Co levels in the alloys. The weight fraction of γ' was reduced from 0.68 for the 3Ta-10W Alloys B, E, and G, to 0.63 for 0Ta-9W Alloys A,

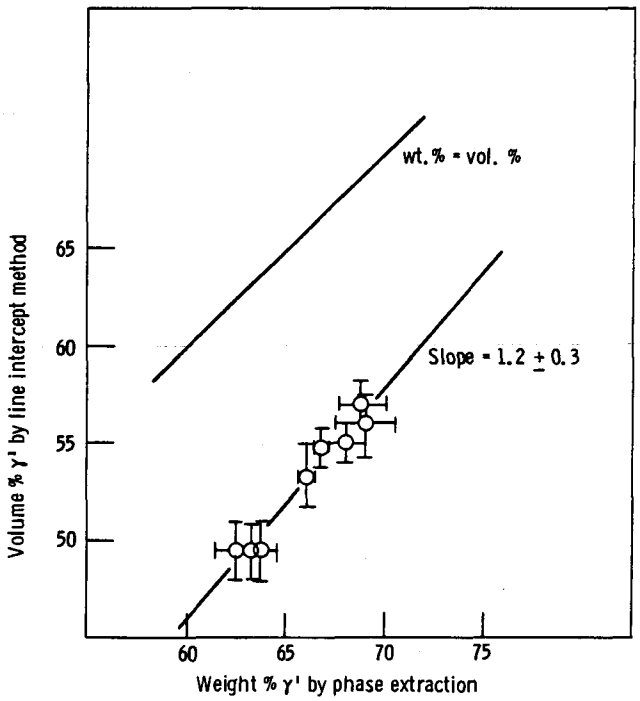

Fig. 4—Comparison of the percentage of γ' phase measured by two techniques.

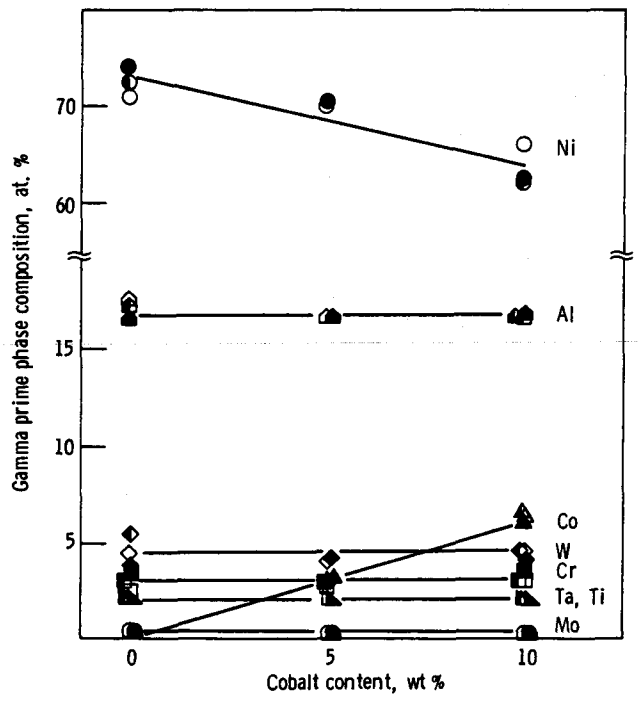

Fig. 5—Composition of the γ' phases of the single crystal alloys. Open, filled, and half-filled symbols correspond to 3Ta-10W, 0Ta-9W, and 0Ta-12W alloys, respectively.

D, and F. Alloys C and H, with 0 pct Ta and 12 pct W, exhibited a γ' weight fraction of 0.66. In addition, the results of quantitative metallography performed on failed rupture specimens are indicated by the closed symbols in Figure 3. The amounts of γ' measured with this technique are lower in magnitude in comparison with the phase extraction technique, although the same trends are apparent as the composition was varied. Again, removal of Ta from the baseline composition caused a decrease in γ' fraction of about 6 vol pct, and replacement of Ta with W caused a reduction of about 3 vol pct. A plot of the amount of γ' measured by the two techniques is shown in Figure 4. The slope of a least-squares line through the data is close to one, which again is indicative of the correspondence of the two methods. However, the data fell significantly below the line drawn for equal measurements by the two techniques. These discrepancies are discussed in more detail in later sections.

The compositions of the γ and γ' phases were determined using phase extraction techniques and are summarized in Table II. The chemical analyses of the extracted γ' residues are illustrated in Figure 5. As Co level in the alloy was decreased from 10 to 0 pct, the Co concentration in γ' decreased from about 6 to 0 at. pct, with a corresponding increase in Ni concentration. The other elements remained relatively constant as the Co, W, and Ta contents were varied. The γ' phase consisted of 17 at. pct Al, 4.5 at. pct W, 3 at. pct Cr, 2 at. pct Ti, and 0.3 at. pct Mo. In the alloys that contained Ta, the γ' phase had 2 at. pct Ta and somewhat lower levels of Ni and Cr.

The γ phase compositions were obtained by analysis of the electrolyte after extraction, and are shown in Figure 6. As a check of the analysis procedures, a mass balance using the amounts and compositions of the two phases can be used to calculate the composition of the bulk sample. Comparison of this calculated composition with the actual chemical analyses of the bulk material revealed that both analysis techniques were in good agreement, with the exception of W and Ta levels. Both the W and Ta levels analyzed in the phase extraction experiments were typically 1 wt pct greater than those measured in the analysis of the bulk material.

Table II. Composition of Phases in the Single Crystal Alloys (At. Pct)

Alloy:	A		B				C		D		E		F		G		H	
Phase:	γ	γ'	γ	γ'	α*	α†	γ	γ'	γ	γ'	γ	γ'	γ	γ'	γ	γ'	γ	γ'
Al	4.46	16.4	5.29	17.4	5.00	0.60	4.43	16.8	4.2	16.6	4.22	16.5	4.63	16.6	4.95	16.4	4.72	16.5
Cr	20.0	3.43	28.6	2.42	25.4	10.6	22.2	3.12	20.2	3.46	24.4	2.75	19.0	3.49	22.4	2.93	21.3	3.13
Co	0	0	0	0	0	0	0	0	8.89	3.36	9.54	2.89	16.4	6.13	17.8	6.28	16.5	6.52
Mo	0.62	0.30	0.89	0.48	5.10	10.2	0.63	0.26	0.59	0.32	0.70	0.34	0.54	0.31	0.53	0.34	0.60	0.28
Ni	72.3	74.2	63.0	70.8	7.50	2.90	69.9	72.5	63.8	70.4	58.6	69.8	57.0	67.5	52.2	65.8	54.0	66.9
Ta	0	0	0	1.98	1.00	1.80	0	0	0	0	0	1.80	0	0	0	1.83	0	0
Ti	0	1.92	0	2.12	0.50	0.30	0	1.92	0	1.94	0	1.96	0	1.95	0	1.93	0	2.01
W	2.49	3.75	1.97	4.44	55.6	73.8	2.72	5.37	2.26	3.94	2.26	3.90	2.21	3.92	1.89	4.53	2.77	4.66

Notes: *Full heat treatment
†Full heat treatment plus 976 hours at 1000 °C

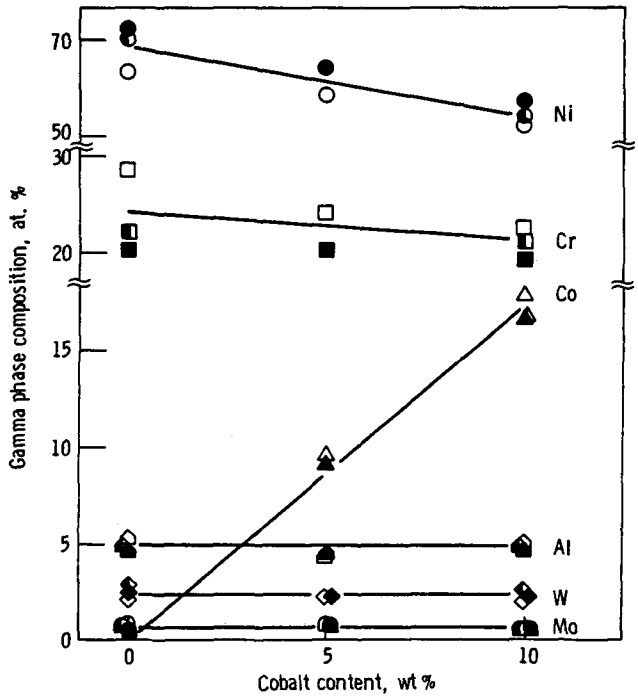

Fig. 6—Composition of the γ phases of the single crystal alloys. Open, filled, and half-filled symbols correspond to 3Ta-10W, 0Ta-9W, and 0Ta-12W alloys, respectively.

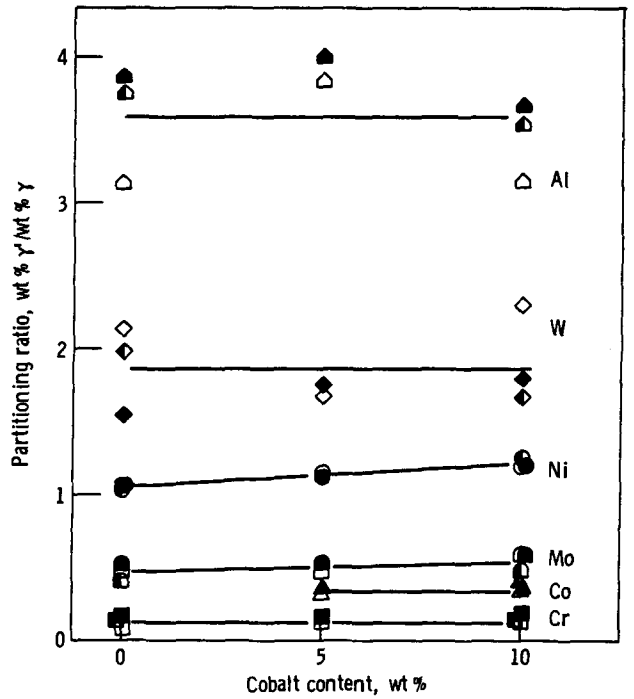

Fig. 7—Partitioning of elements between γ and γ' in the single crystal alloys. Open, filled, and half-filled symbols correspond to 3Ta-10W, 0Ta-9W, and 0Ta-12W alloys, respectively. Values of the ratio for Ta and Ti were essentially infinite.

In comparison to the γ' composition, the composition of the γ phase was more strongly influenced by alloying variations. As Co level in the alloys was decreased from 10 to 0 pct, the Co content in γ decreased from 17 to 0 at. pct and the Ni content increased from approximately 54 to 70 at. pct. In addition, the Cr level increased slightly as Co was removed. Although Al, W, and Mo appeared to remain constant in all the alloys at 5.0, 2.5, and 0.75 at. pct, respectively, the Cr and Ni concentrations varied with the refractory metal content. Removal of the 3 pct Ta and 1 pct W from the baseline caused an increase in Ni by ~5 at. pct and a decrease in Cr by ~4 at. pct. Substitution of the 3 pct Ta by 2 pct W resulted in an increase in Ni of ~4 at. pct and a decrease in Cr of ~2 at. pct.

The partitioning of elements between γ' and γ is represented by the ratio of the concentration of an element in γ' to its concentration in γ. The values for this ratio were essentially independent of the choice of the concentrations in terms of weight or atomic percent. The partitioning ratios are plotted as a function of Co content in Figure 7. Cobalt, Cr, and Mo partition preferentially to the γ phase, with ratios of 0.35, 0.15, and 0.5, respectively. Titanium and Ta partition almost completely to γ', and exhibited partitioning ratios approaching infinity. Although there was some scatter in the ratios for W and Al, no strong trends in the ratio as a function of alloy content were noted, with the average ratios of 1.9 for W and 3.6 for Al. The partitioning ratio of Ni decreased from 1.2 to 1.05 as Co level was decreased from 10 to 0 pct.

In addition to γ and γ', Alloy B had precipitated approximately 0.8 wt pct of W-rich particles. These particles were identified as α-W by X-ray diffraction of extracted residues. The analyzed composition of this phase is also listed in Table II. The results of the γ' extractions of Alloy B should be corrected to account for the presence of α-W in the extracted residue. Accordingly, the weight percent of γ' appearing in Figure 3 is the corrected value. The correction for the composition of γ' did not significantly change the results.

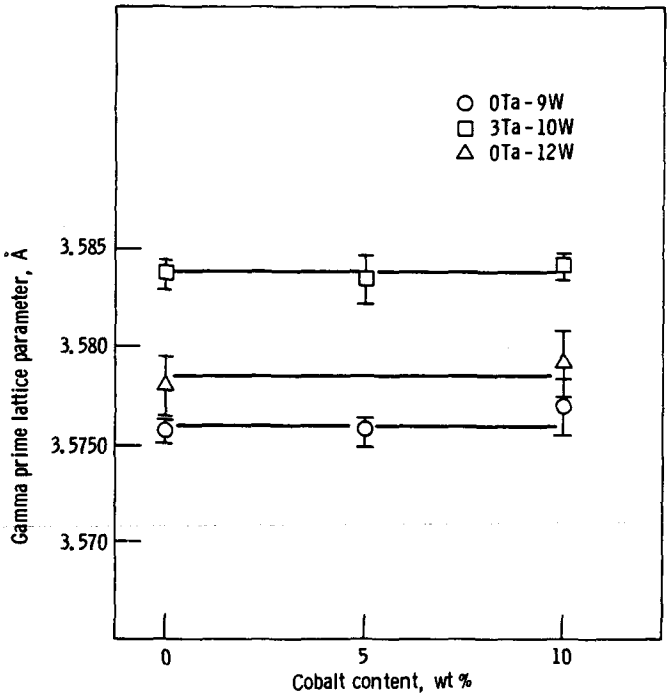

Fig. 8—Lattice parameters of extracted γ' particles in the single crystal alloys.

The lattice parameters of the extracted γ' phases are plotted *vs* composition in Figure 8 and are also listed in

Table III. Room Temperature Lattice Parameter Measurements

Alloy	Full Heat Treatment				Full Heat Treatment Plus 100 Hours at 1000 °C		
	γ' Extracted	γ' *in situ*	γ *in situ*	δ *in situ*	γ' *in situ*	γ *in situ*	δ *in situ*
A	3.5757	3.5754	3.5754	nil	3.5734	3.5734	nil
B	3.5839	3.5849	3.5919	−0.002	3.5831	3.5965	−0.0037
C	3.5780	3.5787	3.5787	nil	3.5735	3.5817	−0.0023
D	3.5757	3.5752	3.5752	nil	3.5744	3.5744	nil
E	3.5835	3.5842	3.5842	nil	3.5804	3.5804	nil
F	3.5771	3.5772	3.5772	nil	3.5746	3.5746	nil
G	3.5842	3.5843	3.5843	nil	3.5818	3.5818	nil
H	3.5792	—	—	nil	3.5780	3.5780	nil

Table III. These results are representative of the unconstrained γ' lattice parameter. Figure 8 illustrates that the γ' lattice parameter was not affected by Co level, but was dependent on the Ta and W contents in the alloys. The baseline 3Ta-10W alloys had $a\gamma' = 3.5840$ Å, whereas the 0Ta-9W alloys had $a\gamma' = 3.5760$ Å and the 0Ta-12W alloys had $a\gamma' = 3.5785$ Å.

The *in situ* lattice parameters of the γ and γ' phase were measured at room temperature by a diffractometer scan of the [420] peaks from oriented single crystals, which were examined both in the heat treated condition and also after aging for 100 hours at 1000 °C. These results are listed in Table III. With the exception of Alloy B, the difference between the extracted and *in situ* lattice parameters was smaller than the experimental scatter. The decrease in lattice parameters observed after aging was significant, and had some influence on the lattice mismatch. The lattice mismatch between the γ and γ' phases, δ, is defined as:

$$\delta = 2(a\gamma' - a\gamma)/(a\gamma' + a\gamma) \qquad [1]$$

where $a_{\gamma'}$ and a_{γ} are the lattice parameters of the two phases. Before aging, only Alloy B exhibited a value of δ large enough to measure. After the 100-hour age, the magnitude of δ for Alloy B increased from about −0.002 to −0.0037, and for Alloy C, the magnitude increased from approximately zero to −0.002. Typical X-ray peaks after an aging for 100 hours at 1000 °C are illustrated in Figure 9. For Alloy B, which possessed the highest value of δ, the γ and γ' peaks were clearly resolved, as shown in Figure 9(a). Removal of Ta from Alloy B to form Alloy A reduced the mismatch to below the resolution limit, Figure 9(b). Similarly, addition of 5 pct Co to Alloy B to form Alloy E also reduced the magnitude of δ, as presented in Figure 9(c). The [420] peaks for Alloy C, the only other alloy which possessed a value of δ large enough to measure, are presented in Figure 9(d).

3. *Microstructure after long aging treatments*

The thermal stability of the alloys was investigated by isothermal aging at elevated temperatures. The effect of aging on the lattice parameters was discussed in the previous section. Other changes in microstructure were also examined, including γ' coarsening, loss of coherency, and precipitation of third phases. The γ' particles coarsened appreciably during aging at 1000 °C. Microstructures of Alloy A after aging for times approaching 1000 hours are presented in Figures 10(a) through (d). The coarsening particles of all alloys followed the typical $t^{1/3}$ time dependence. mine the rate constant, k, for coarsening.

$$(\bar{a}/2)^3 - (\bar{a}_0/2)^3 = kt \qquad [2]$$

Here $\bar{a}_0$ and $\bar{a}$ are the average lengths of a γ' cube edge at times zero and t, respectively. The rate constant k is plotted *vs* composition in Figure 11, which illustrates that removal of Co from these alloys approximately doubles the coarsening rate. The coarsening rates for Alloys B and C are also plotted in Figure 11, although these data cannot be directly compared to the other rates. The γ' particles of these two alloys assumed irregular or plate-like morphologies during the aging treatment, and the coarsening rates of these two alloys are affected by the choice of the particle dimension to be measured. This change in shape appeared to be related to a loss of coherency, as evidenced by the dislocation networks imaged in Figure 2. In addition, the presence of misfit dislocations alters the coarsening rate,[9] and thus comparison of alloys having semi-coherent γ' particles with those in which the γ' particles remained coherent may not be justified.

The presence of W-rich precipitates is also illustrated in Figure 12. There were both acicular and blocky particles evident in Alloy B, and *in situ* EDAX analysis in the SEM revealed that both types of particles were rich in W. X-ray diffraction of extracted residues showed that these precipitates were mainly α-W with trace amounts of μ phase. Aging Alloy B for 976 hours at 1000 °C increased the amount of W-rich phases from 0.8 to 3.7 wt pct. Aging Alloy C increased the amount of W-rich phases from zero to 0.5 wt pct. The addition of Co to form Alloys D to H or the reduction of the Ta plus W total to form Alloy A eliminated the formation of these phases.

4. *Microstructure after creep-rupture testing*

Creep-rupture testing of the alloys was performed at 925 and 1000 °C, and the results of these tests are presented in the companion paper.[6] After creep-rupture testing at these temperatures, the γ' particles of all alloys had coarsened from their initial cubic or spherical morphology to lamellae perpendicular to the applied stress. Typical scanning electron micrographs of several alloys are presented in Figures 13(a) through (d). These photographs were also used for quantitative metallographic determination of γ' volume fraction, presented previously in Figure 3. The lamellar structure is more uniform and more well defined than the distribution of cubic γ' particles, and thus is more amenable to the use of the line intercept technique. Furthermore, the measurements on creep-rupture tested samples appeared to be more representative of the γ' volume fraction

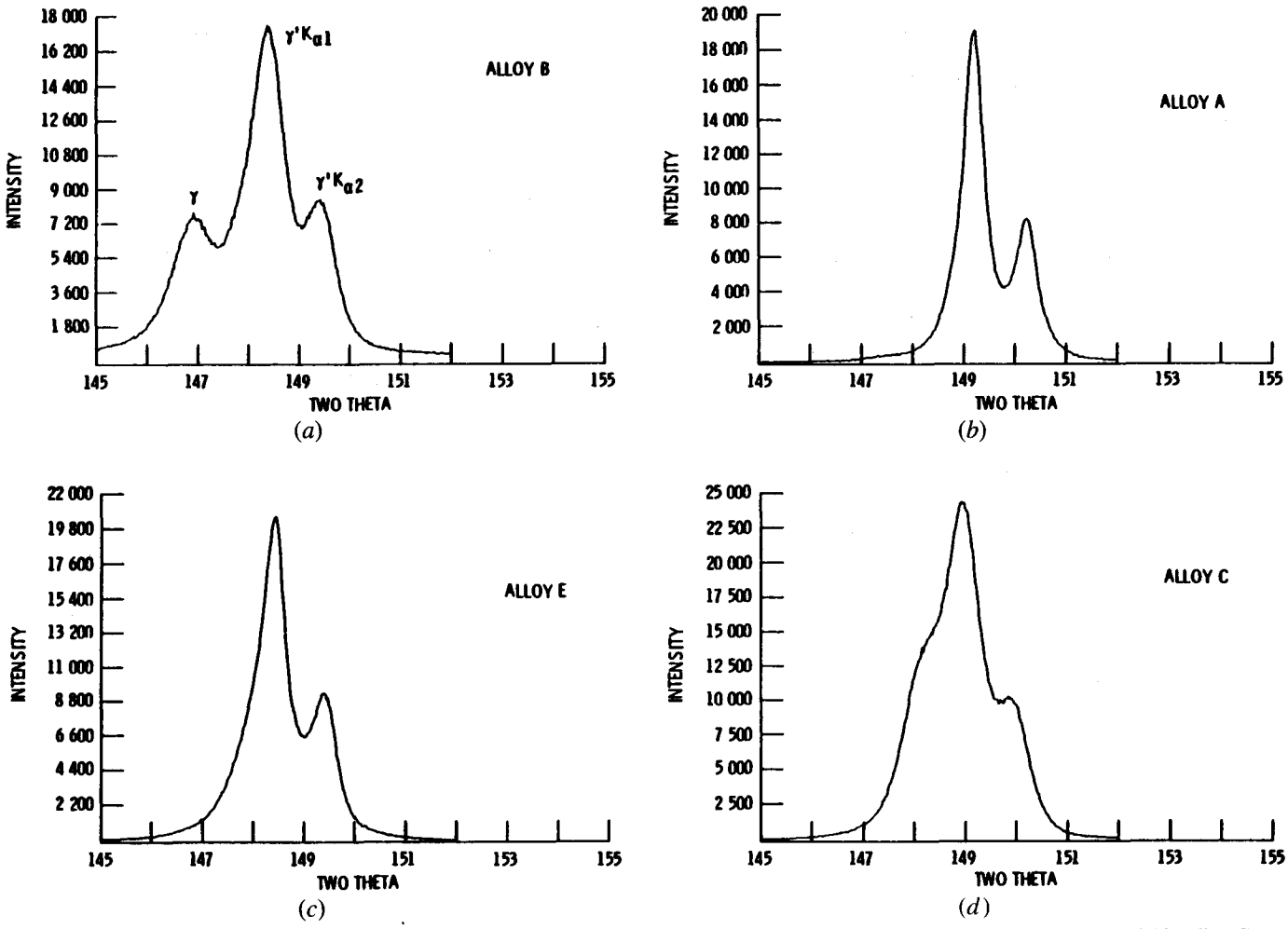

Fig. 9—Diffractometer scans of the (420) peaks from bulk samples of single crystal alloys. (*a*) Alloy B, (*b*) Alloy A, (*c*) Alloy E, and (*d*) Alloy C.

at the testing temperature. Most of the γ' that precipitated during cooling from the creep testing temperature would be in the form of fine spherical precipitates, and thus could be easily distinguished from the lamellar γ'. This fine cooling γ' would be included in the amount of γ' measured by the phase extraction technique, which therefore is a measurement of the total γ' content at room temperature. Alloy B, which was creep tested at several temperatures, provided data for the temperature dependence of the γ' volume fraction in this range. The γ' volume fractions of Alloy B at the various testing temperatures, along with the room temperature phase extraction measurement and the DTA solvus measurement, are plotted *vs* temperature in Figure 14; similar data for UDIMET 700[10] and RENÉ*95[11] are also shown on the figure.

*RENÉ is a trademark of General Electric Company.

The γ' coarsening behavior during creep was examined in detail for Alloy B, and was presented previously.[12] Briefly, the γ' particles coalesced into lamellae in the absence of any lamellar thickening. This process was very rapid at 1000 °C, typically occurring during the primary creep stage. After prolonged creep exposure, thickening of the lamellar structure was evident. The kinetics of oriented coarsening in the other alloys was also studied, and micrographs of samples tested at 1000 °C and 148 MPa are shown in Figures 15(a) through (d). These micrographs demonstrate that the γ' coarsening was a function of composition as well as temperature and stress. The γ' plate formation in Alloy C was similar to that in Alloy B, as illustrated in Figures 15(a) and (b). However, this coarsening was significantly slower in Alloys E and F, as exhibited in Figures 15(c) and 15(d), respectively.

Finally, a few creep tested specimens were examined by TEM. Figure 16(a) is a transverse section from a specimen of Alloy B creep tested at 1000 °C and 148 MPa for 45.8 hours, which is close to the onset of steady state creep. This micrograph shows the hexagonal array of misfit dislocations located at the γ-γ' interface. With the operative g-vector of 200, only two of the three sets of dislocations which make up the network are imaged in Figure 16(a). Figure 16(b) is a transverse section from a specimen of Alloy E creep tested at 1000 °C and 148 MPa for 60.3 hours. The misfit dislocation spacings were considerably greater in Alloy E, reflecting the lower γ-γ' mismatch of this alloy compared to that of Alloy B (Figure 16(a)).

B. *Discussion*

The primary microstructural feature in all of the single crystal alloys is the copious precipitation of the γ' phase. Measurements of particle size were fit to Eq. [2] to deter-

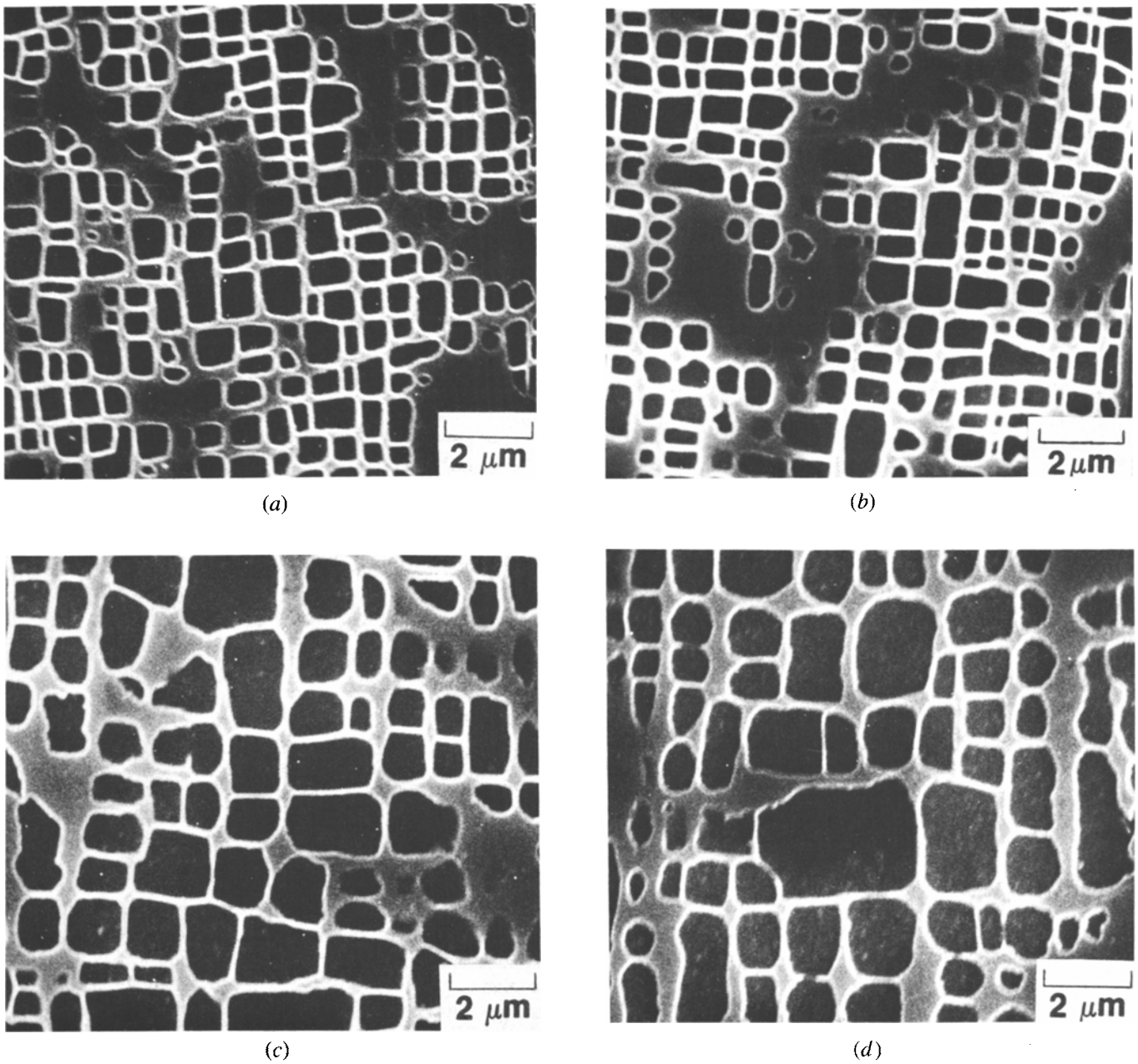

Fig. 10—Scanning electron micrographs of Alloy A after aging at 1000 °C for various times. (*a*) 95.3 h, (*b*) 215.4 h, (*c*) 479.4 h, and (*d*) 976.0 h.

The influence of composition on the solvus, particle size, particle shape, volume fraction, lattice parameter, and coarsening rates of the γ' phase will be emphasized in the discussion below. Again, keep in mind that the W concentrations were slightly lower than the aim compositions in the alloys where Ni or W was substituted for the baseline Ta content.

1. *Transformation temperatures*

The influence of Co, Ta, and W contents on the transformation temperatures of these alloys is important for the determination of proper solution treatment temperatures. Optimum mechanical properties are obtained when the coarse γ' present in the as-cast microstructure is completely dissolved and reprecipitated as a fine dispersion. The large difference between the solidus and the γ' solvus enabled all alloys to be properly solution treated. The increase in γ' solvus as Co content was decreased from 10 to 0 pct is consistent with previous results.[3,5,7] The decrease in solvus which resulted from the removal of Ta was expected because Ta partitions strongly to the γ' phase. Substitution of W for Ta produced an intermediate reduction of the solvus, consistent with the tendency of W to partition less strongly to γ'. The solvus temperatures of the alloys were also correlated with the volume fraction of γ'. High levels of elements which partition strongly to γ' promote higher volume fractions of γ' and increase the stability of γ', which results in increased γ' solvus temperatures. Tantalum is a strong γ' former and therefore the 3Ta-10W alloys exhibited the highest solvus temperatures and the highest percentage of γ'. Tungsten partitions less strongly to γ', and the 0Ta-12W alloys had lower γ' solvus temperatures and γ' fractions.

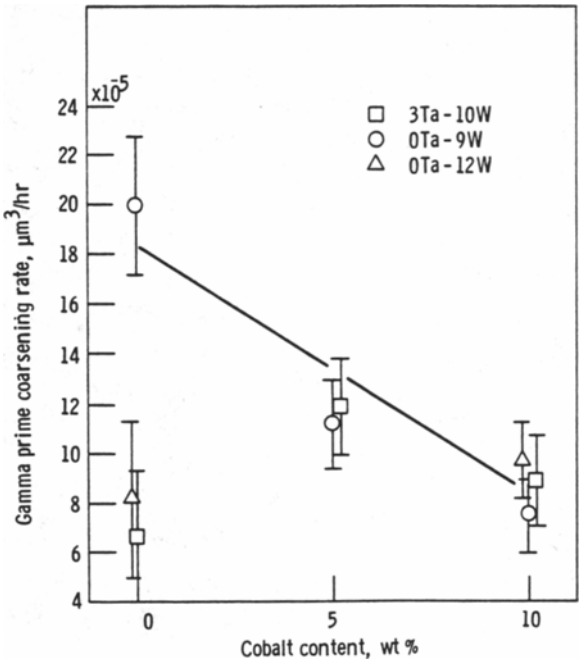

Fig. 11—Gamma prime coarsening rates for the single crystal alloys at 1000 °C.

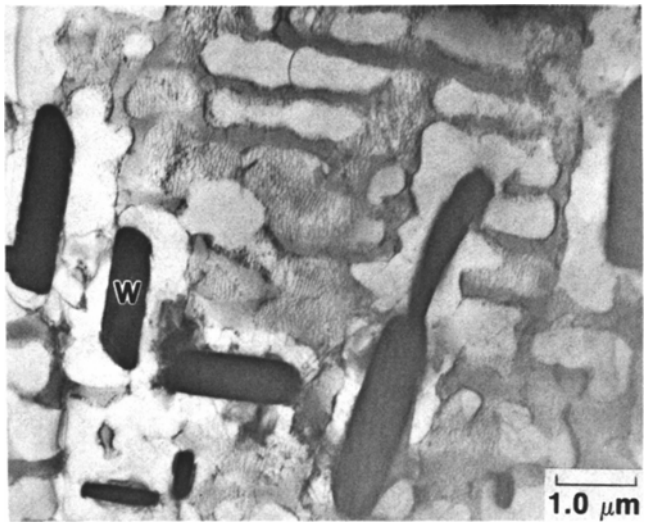

Fig. 12—Transmission electron micrograph of Alloy B aged for 976 h at 1000 °C. Note the irregular γ' morphology, extensive dislocation networks, and αW precipitates.

The 0Ta-9W alloys, with the lowest Ta plus W totals, also had the lowest solvus temperatures and γ' fractions. However, there were some exceptions to the general correlation between solvus and γ' fraction, as illustrated by the influence of Co level; the Co content had a strong effect on the γ' solvus but did not significantly affect the percentage of γ'.

2. *Gamma prime fraction*

The weak influence of Co on the γ' volume fraction is similar to results reported previously in other alloys,[4,5] where only small decreases in γ' fraction as the Co content was decreased were observed. The work on polycrystalline MAR-M247[3] appears to be the only study to report significant changes in γ' fraction as a function of Co level. Although there are no apparent reasons for this effect, the lack of confirmation of the results gives reason to doubt the phase extraction data in Reference 3.

As presented in Figures 3 and 4, the two methods used for measurement of γ' fraction produced similar trends, but were significantly different in magnitude. The weight fraction measurements obtained from phase extraction should be converted to volume fraction for direct comparison to the quantitative metallographic results. This correction did not change the phase extraction results significantly, based on the calculated densities of the γ and γ' phases, which were based on published regression equations.[13] The equality of the densities is also in agreement with other workers.[10] These results imply that the observed differences between the γ' fraction determined by the two methods cannot be rationalized by differences in the densities of γ and γ'. As discussed previously, the γ' fraction measured by quantitative metallography on failed creep-rupture specimens is more representative of the γ' fraction at the testing temperature, whereas the phase extraction results should be representative of the γ' fraction at room temperature. The temperature dependence of the γ' fraction is reasonable in comparison to previous work.[10,11] Consequently, it is concluded that the observed differences in γ' fraction measured by the two methods is primarily the result of the difference in γ' fraction at room temperature and at the creep testing temperature.

3. *Gamma prime morphology*

In the fully heat treated condition, the γ' particles are present as a fine distribution of discrete particles. Although the size of the particles did not vary significantly as composition was varied, the shape of the particles was a function of the alloy content. Some of the alloys, such as Alloys A, D, F, and G, possessed spherical particles, which is typical for alloys with low γ-γ' mismatch and small particle sizes.[14] Other alloys, such as Alloys B, C, E, and H, exhibited cuboidal γ' morphologies, consistent with higher mismatch values. The γ' phase which was in the form of spherical particles underwent a transition to a cuboidal morphology upon subsequent aging, as seen for Alloy A in a comparison of Figures 2(a) and 10(a). This commonly observed effect[15,16] has been explained as a consequence of a balance between surface and elastic strain energies in γ-γ' systems. At sufficiently large particle sizes, this effect more than compensates for the increase in surface area in changing from spherical to cuboidal particles.

4. *Phase compositions*

The chemical analyses of the γ and γ' phases produced some interesting results. As expected, the concentration of Co decreased and that of Ni increased in the γ' phase as Ni was substituted for Co in the bulk alloys. Similarly, the Ta containing alloys exhibited high Ta concentrations in γ'. Apart from these changes, any trends in the concentrations of the other elements in γ' were smaller than the experimental scatter. These data do indicate that the γ' phase contains significant amounts of W, Ti, and Ta in solid solution. The composition of the γ phase varied slightly as a function of the bulk alloy composition. In addition to the expected changes in Co and Ni contents as the total Co level was varied, the Cr, W, and Ni concentrations varied slightly

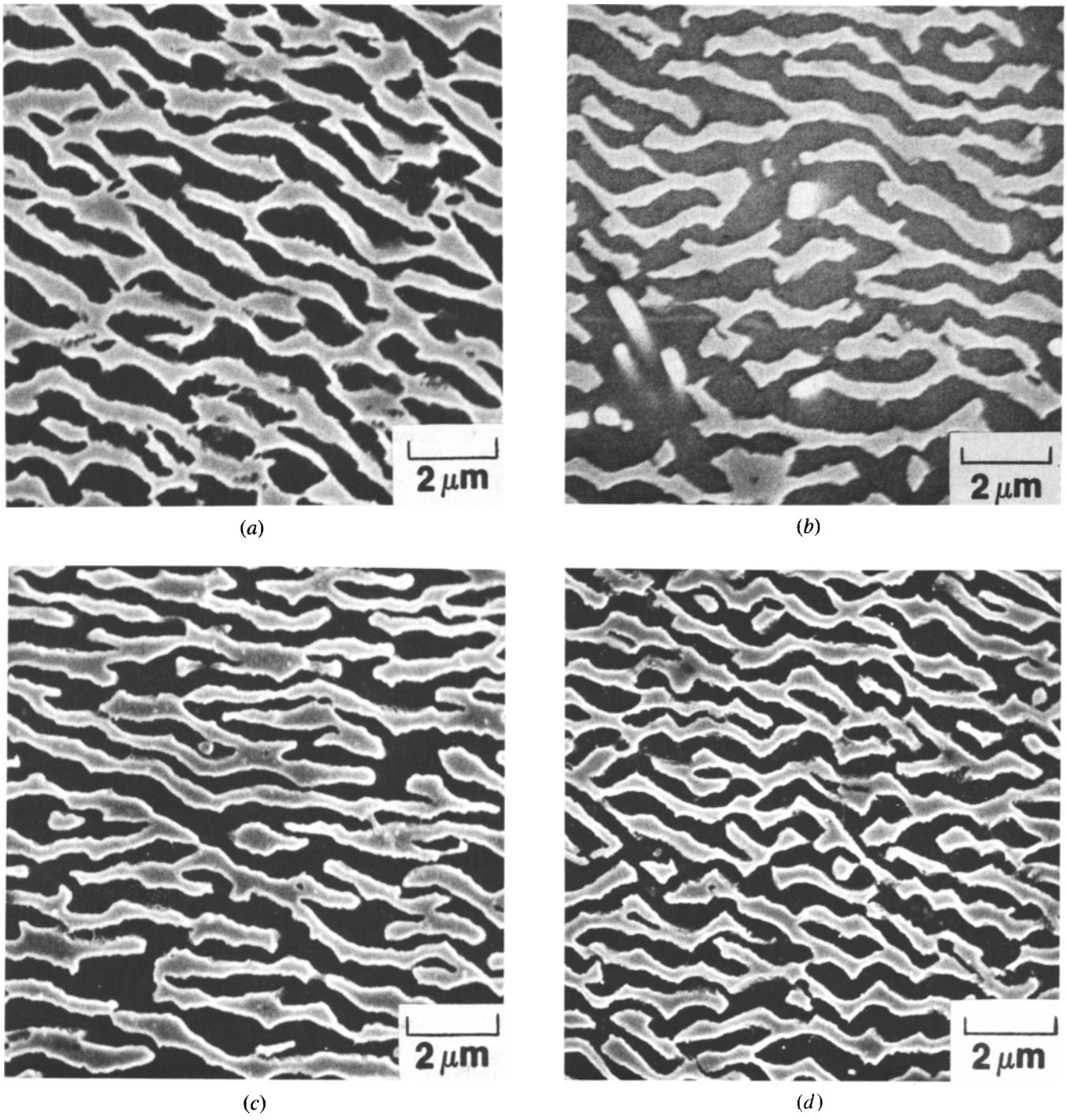

Fig. 13—Scanning electron micrographs of longitudinal sections of failed creep-rupture specimens. (*a*) Alloy A, t = 110 h, e = 30 pct; (*b*) Alloy B, t = 110 h, e = 20 pct; (*c*) Alloy E, t = 91 h, e = 20 pct; (*d*) Alloy C, t = 383 h, e = 13 pct, where t and e are the time and elongation at failure, respectively. Micrographs were taken in areas away from the fracture surface. Stress axis is vertical in all photos.

with both Co and refractory metal levels in the bulk alloy. The above changes in γ and γ' compositions are reflected in the partitioning ratios of the individual elements. The partitioning of elements was not significantly influenced by the various alloying modifications. In agreement with previous work,[17] Cr, Co, and Mo partition preferentially to the γ phase, whereas Al, Ti, and Ta partition to γ'. The W partitioning ratio appears to be high in comparison to results on similar alloys, where it was found that W partitioned approximately equally between γ and γ'.[17,18,19] One source for this discrepancy is the uncertainty in the chemical analysis for W in the present results.

It is apparent that both the γ matrix and the γ' precipitate are highly alloyed. The γ phase has significant amounts of Cr, Co, Al, W, and Mo, and γ' contains W, Ti, Ta, Co, Cr, and Mo. In fact, the concentrations of elements in the γ and

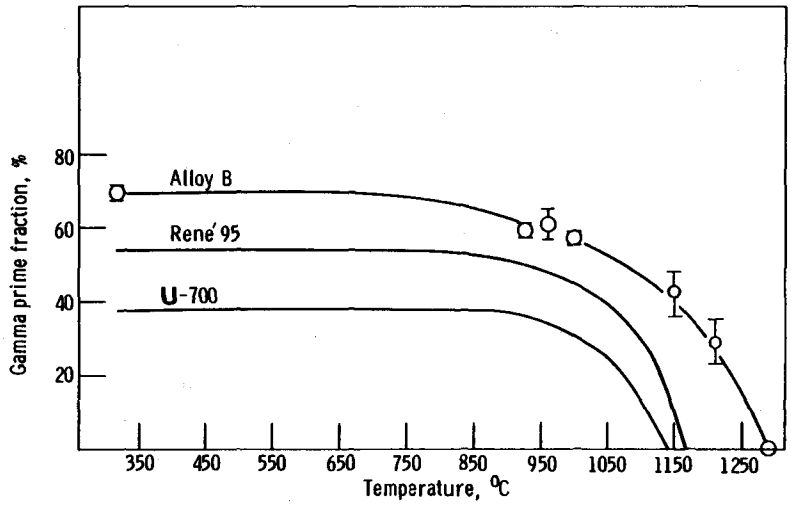

Fig. 14—Temperature dependence of γ' volume fraction of Alloy B, UDIMET 700,[11] and RENÉ 95.[12]

γ' have approached and even reached the solid solubility limit, as evidenced by the small amounts of W-rich precipitates in Alloys B and C. These elements, especially the refractory metals W and Ta, are expected to have significant contributions to solid solution strengthening mechanisms. In addition, as the solid solubility limits for these elements are approached, the influence of short range order may contribute to the strength of these alloys.[20]

As mentioned above, precipitation of the W-rich phases α and μ were observed in Alloys B and C. The amount of these phases is dependent on the total Ta plus W level, as well as the Co level in the alloy. Alloy B, with 13 pct of Ta plus W, exhibited the largest amount of W-rich precipitates. Alloy C, with 12 pct of Ta plus W, precipitated only a small amount. Finally, Alloy A, with only 9 pct of Ta plus W, did not exhibit any third phase precipitation. The addition of 5 pct Co to Alloy B, which formed Alloy E, also eliminated the α and μ precipitation. This is in agreement with previous results which have shown increases in the solubility for W in the γ-γ' matrix as Co was increased.[7] Although the influence of Co on the solubility of W is clearly shown in this investigation by the absence of W-rich phases in Alloy E, the increased W concentrations were not observed in the chemical analyses of the γ and γ' phases. Evidently, the magnitude of the expected changes was below the sensitivity limits of the chemical analysis procedures.

5. *Lattice mismatch*

The lattice parameter measurements also provided important information. The γ' lattice parameters were independent of Co content, which is consistent with the analyzed composition of γ'. As Co content was increased, only the Co and Ni concentrations in γ' changed. Since Co and Ni have only very small differences in atomic size, the lattice parameter of γ' would not be expected to vary significantly.[21] The alloys with high W or Ta levels exhibited higher lattice parameters, as expected from the large atomic radii of these elements. The difference between the constrained and unconstrained γ' lattice parameters was negligible for all alloys except Alloy B. Alloy B, with the highest lattice misfit, would be expected to exhibit the largest constraint on the lattice parameter, which in turn would result in the largest difference between the extracted and *in situ* measurements. The decrease in lattice parameters which resulted from the 100-hour age at 1000 °C indicates that the compositions of γ and γ' were changing during the aging treatment. Some of these changes in composition could have resulted from a reduction of residual dendritic segregation, although this effect would be very small at such a low temperature. Another possible source for the changing composition is that the compositions are gradually approaching their local equilibrium value.

The lattice misfit between the γ and γ' phases is expected to have significant influences on the properties of these alloys. As displayed in Table III, only the alloys with 0 pct Co and high Ta plus W levels had room temperature misfit values large enough to be measured by X-ray diffraction. The addition of 5 pct Co was sufficient to decrease the misfit to below the detection limit. Because the γ' lattice parameter was independent of Co content, the effects of Co on mismatch were accomplished by changes in the γ lattice parameter. A decrease in the magnitude of the lattice mismatch as Co level increased was also noted in other work,[16] although these latter alloys possessed positive misfit values. Although Co is not expected to alter the lattice parameter of Ni very significantly,[21] its effects on the concentration of other elements in the γ phase may account for the changes in lattice parameter of γ. The 100-hour age at 1000 °C also increased the magnitude of the measured lattice mismatch for Alloys B and C. This effect can be explained by the loss of coherency exhibited in these alloys. The presence of misfit dislocations would consume the elastic coherency strains, thereby relieving the constraint on the lattice parameters, and thus increasing the measured mismatch. In another study,[22] it was shown that the magnitude of the mismatch measurement for Alloy E was also increased after coherency was lost. For Alloy E, creep exposure to form a lamellar γ' structure was necessary to produce a semicoherent interface.

Finally, it should be noted that the value of lattice mismatch at room temperature can vary significantly from the value at elevated temperature. The mismatch values of these alloys is expected to tend toward more negative values as the temperature is increased.[22–25]

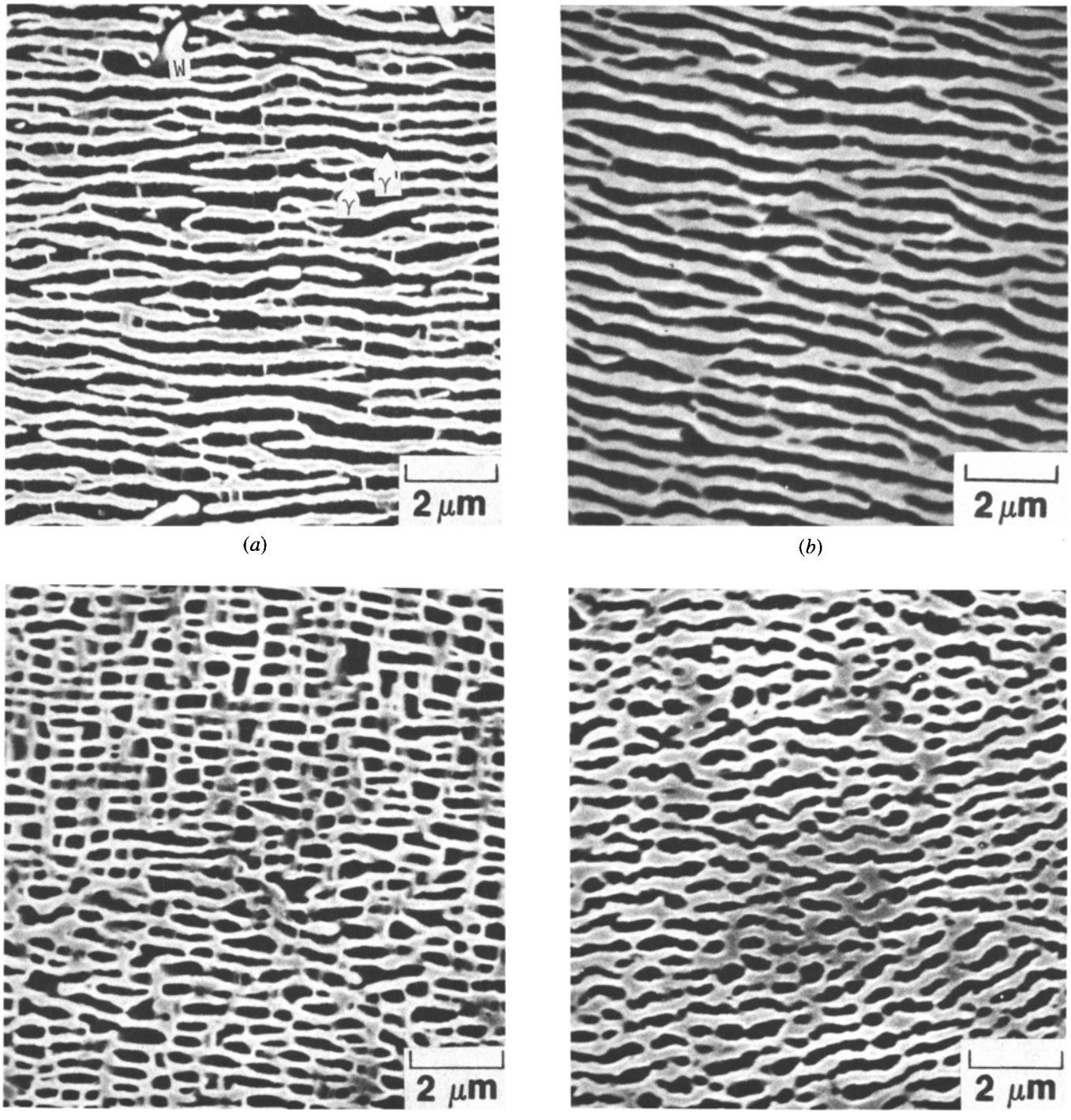

Fig. 15—Longitudinal microstructures of samples creep tested at 1000 °C and 148 MPa. (*a*) Alloy B, t = 20 h, ε = 0.6 pct; (*b*) Alloy C, t = 30 h, ε = 0.7 pct; (*c*) Alloy E, t = 20 h, ε = 0.3 pct; (*d*) Alloy F, t = 20 h, ε = 0.6 pct, where t and ε are the accumulated time and strain for each interrupted test. Stress axis is vertical in all photos.

6. *Gamma prime coarsening*

Exposure at 1000 °C for extended periods of time resulted in changes in γ and γ' chemistries, γ' coarsening, precipitation of W-rich phases, and loss of coherency. For the alloys with γ' particles that remained coherent, reduction in Co level increased the γ' coarsening rate. This effect is consistent with previous findings.[16] The reasons for this effect are unclear, as it appears that Co additions may influence several factors that may decrease γ' coarsening rates, such as diffusion or mismatch. One unexpected result was the lack of any effect of refractory metal levels on γ' coarsening rates. It was expected that alloys with higher levels of the slower diffusing Ta and W would have lower γ' coarsening rates, but evidently the magnitude of the compositional changes was not sufficient to cause the expected reductions in coarsening rates.

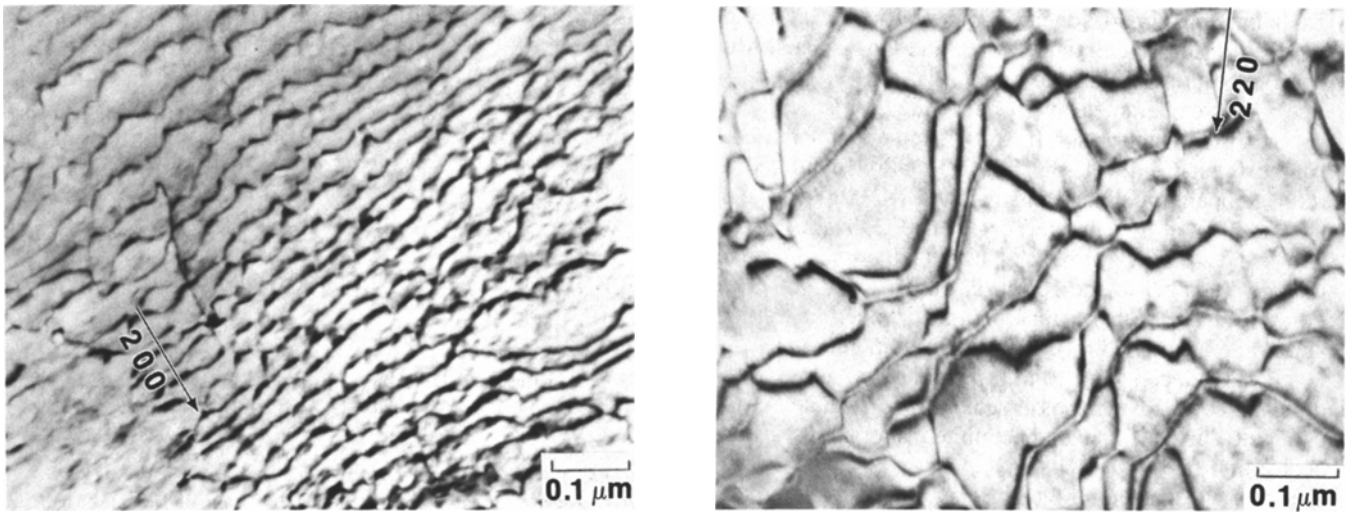

(*a*) (*b*)

Fig. 16—Transverse sections of samples creep tested at 1000 °C and 148 MPa, illustrating the hexagonal array of misfit dislocations. (*a*) Alloy B, 45.8 h; (*b*) Alloy E, 60.3 h.

As discussed previously, the 0 pct Co Alloys B and C were exceptions to the above trends and exhibited anomalously low coarsening rates. These low rates appear to be the result of the loss of coherency which occurred in these two alloys. Because of their high lattice mismatches, Alloys B and C exhibited a loss in coherency at smaller particle sizes and shorter times than the other alloys. Although some workers have reported increased coarsening rates when coherency was lost,[9,26] other data appear to support the opposite conclusion, whereby a stabilization against particle growth at long aging times was reported.[27,28] This stabilization was associated with the loss of coherency in a Cu-Co alloy.[28] Although no conclusive reasons for the stabilization were given by Footner and Richards,[27] they did observe an irregular γ' morphology associated with this phenomenon. A change from a cuboidal to irregular γ' morphology as an indication of loss of coherency is consistent with this investigation and the observations in Reference 29. Thus, it is reasonable to associate the stabilization of γ' size observed by Footner and Richards with a loss of coherency, in agreement with the interpretation of Porter *et al.*[30] It also follows that the low γ' coarsening rates observed in this study can also be attributed to the loss of coherency. One possible mechanism for this effect is that the stable misfit dislocation network may decrease the mobility of the γ-γ' interface, which could decrease the coarsening rate.[31] The observation that alloys with higher γ-γ' mismatch values exhibited lower γ' coarsening rates is contrary to the ideas of some workers,[32,33] but in agreement with the results of others.[34,35,36] However, it is recognized that except as noted above, the loss of coherency was not observed in these other studies.

Unstressed aging of most of the alloys did not result in any γ' plate formation. However, the γ' precipitates in the alloys with higher mismatch, Alloys B and C, did exhibit a tendency for coalescence into plate-like morphologies oriented on cube planes. The application of a stress not only greatly enhances the tendency to coalesce but also provides a bias for coalescence on a single (001) plane. All alloys exhibited pronounced directional coarsening during creep testing at 1000 °C. Although the mismatch values of most of the alloys were unmeasurably small, the observation that all alloys formed γ' lamellae normal to the applied stress supports the conclusion that all alloys had negative δ values at the testing temperature.[22–25,37] The rate of directional coarsening at a given applied stress and temperature correlated with the magnitude of δ measured at room temperature. Alloys B and C, with the largest magnitude of δ, exhibited the most rapid γ' plate formation, whereas, Alloys E and F, with smaller δ values, exhibited significantly slower directional coarsening. This can be explained by the concept that an increase in the magnitude of lattice mismatch causes an increased driving force and thus more rapid coarsening. It should be noted, however, that even for the alloys with low mismatch, the directional coarsening was still rapid. For example, Alloy E exhibited the fully developed lamellar structure after approximately 60 hours, and a rupture life of about 600 hours at 1000 °C and 148 MPa. Thus, the fully formed lamellae were present for about 90 pct of the rupture life.

Thus, the Co, Ta, and W variations resulted in significant changes in microstructural features such as γ' volume fraction, γ' morphology, γ-γ' lattice mismatch, γ' coarsening, and the presence of third phases. These microstructural features can have a pronounced effect on the mechanical properties of these alloys, as will be discussed elsewhere.[6]

IV. SUMMARY

1. Removal of Ta and W from the baseline 3Ta-10W alloys to form the 0Ta-9W alloys caused large reductions in γ' solvus temperature and γ' volume fraction. Substitution of W for Ta to form the 0Ta-12W alloys resulted in intermediate reductions in solvus temperature and volume fraction. The amount of γ' was independent of Co level, although the γ' solvus temperature increased significantly as Co content was reduced from 10 to 0 pct.
2. The partitioning of elements between the γ and γ' phases did not vary appreciably as the alloy composition varied.

Tantalum and Ti partitioned almost totally to γ'; Al and W partitioned preferentially to γ'; and Co, Cr, and Mo partitioned preferentially to γ.

3. The γ' lattice parameter was independent of Co content but increased as the total refractory metal level increased. At the 0 pct Co level, the 3Ta-10W alloy exhibited a room temperature lattice mismatch $\delta = -0.0037$, and the 0Ta-12W alloy exhibited $\delta = -0.002$. The 0Ta-9W alloys and all alloys with 5 and 10 pct Co possessed mismatch values below the detection limit.
4. For the alloys with γ' that remained coherent during aging, the unstressed γ' coarsening rate increased as Co level was reduced from 10 to 0 pct. The two alloys with high lattice mismatch possessed γ' that became semicoherent during aging and exhibited anomalously low coarsening rates.
5. Oriented γ' coarsening which resulted in lamellae perpendicular to the applied stress was very prominent during creep. Alloys with higher magnitudes of lattice mismatch exhibited faster directional coarsening rates and a finer spacing of misfit dislocations at the γ-γ' interfaces.

ACKNOWLEDGMENTS

This work was partially supported by NASA Grant NSG 3-30. The authors would like to thank Dr. R. A. MacKay and Mr. R. G. Garlick of NASA Lewis Research Center and Mr. Joseph Doychak of Case Western Reserve University for useful discussions and technical assistance.

REFERENCES

1. J. K. Tien, T. E. Howson, G. L. Chen, and X. S. Xie: *J. Metals*, Oct. 1980, vol. 32, p. 12.
2. M. V. Nathal, R. D. Maier, and L. J. Ebert: *Metall. Trans. A*, 1982, vol. 13A, p. 1775.
3. M. V. Nathal, R. D. Maier, and L. J. Ebert: *Metall. Trans. A*, 1982, vol. 13A, p. 1767.
4. G. E. Mauer, L. A. Jackman, and J. Domingue: in *Proc. 4th Intl. Symp. on Superalloys*, J. K. Tien, S. T. Wlodek, H. Morrow, M. Gell, and G. E. Mauer, eds., ASM, Metals Park, OH, 1980, p. 43.
5. R. N. Jarrett and J. K. Tien: *Metall. Trans. A*, 1982, vol. 13A, p. 1021.
6. M. V. Nathal and L. J. Ebert: *Metall. Trans. A*, 1985, vol. 16A, p. 1863.
7. T. E. Strangman, G. S. Hoppin, C. M. Phipps, K. Harris, and R. E. Schwer: in *Proc. 4th Intl. Symp. on Superalloys*, J. K. Tien, S. T. Wlodek, H. Morrow, M. Gell, and G. E. Mauer, eds., ASM, Metals Park, OH, 1980, p. 215.
8. M. J. Donachie and O. H. Kriege: *J. Mat.*, 1972, vol. 7, p. 269.
9. P. K. Rastogi and A. J. Ardell: *Acta Metall.*, 1971, vol. 19, p. 321.
10. E. H. VanDerMolen, J. M. Oblak, and O. H. Kriege: *Metall. Trans.*, 1971, vol. 2, p. 1627.
11. R. L. Dreshfield: NASA TMX-73663, 1977, National Technical Information Services, Springfield, VA 22161.
12. M. V. Nathal and L. J. Ebert: *Metall. Trans. A*, 1985, vol. 16A, p. 427.
13. F. C. Hull: *Metal Progress*, 1969, vol. 96, p. 139.
14. W. T. Loomis, J. W. Freeman, and D. L. Sponseller: *Metall. Trans.*, 1972, vol. 3, p. 989.
15. A. J. Ardell and R. B. Nicholson: *J. Phys. Chem. Solids*, 1966, vol. 27, p. 1793.
16. C. K. L. Davies, P. Nash, and R. N. Stevens: *J. Mat. Sci.*, 1980, vol. 15, p. 1521.
17. O. H. Kriege and J. M. Barris: *Trans. ASM*, 1962, vol. 62, p. 195.
18. P. Caron and T. Khan: *Mat. Sci. Eng.*, 1983, vol. 61, p. 173.
19. H. C. Nguyen, B. J. Pletka, and R. W. Heckel: in *High Temperature Alloys: Theory and Design*, J. O. Stiegler, ed., AIME, Warrendale, PA, 1984, p. 381.
20. E. Aigeltinger and M. Kersker: *Metals Forum*, 1981, vol. 4, p. 112.
21. W. B. Pearson: *Handbook of Lattice Spacings and Structures of Metals*, Pergamon Press, New York, NY, 1959, vols. 1, 2, p. 776.
22. M. V. Nathal, R. A. MacKay, and R. G. Garlick: *Mat. Sci. Eng.*, in press.
23. D. A. Grose and G. S. Ansell: *Metall. Trans. A*, 1981, vol. 12A, p. 1631.
24. T. Khan, P. Caron, and C. Duret: in *Superalloys 1984: Proc. Fifth Int. Symp. on Superalloys*, M. Gell, C. S. Kortovich, R. H. Bricknell, W. B. Kent, and J. F. Radavich, eds., AIME, Warrendale, PA, 1984, p. 145.
25. A. Fredholm and J. L. Strudel: in *Superalloys 1984: Proc. Fifth Int. Symp. on Superalloys*, M. Gell, C. S. Kortovich, R. H. Bricknel, W. B. Kent, and J. F. Radavich, eds., AIME, Warrendale, PA, 1984, p. 211.
26. R. B. Nicholson: in *Interfaces Conference*, R. C. Gifkins, ed., Aust. Inst. Metals, Melbourne, Australia, 1969, p. 139.
27. P. K. Footner and B. P. Richards: *J. Mat. Sci.*, 1982, vol. 17, p. 2141.
28. J. W. Martin and F. J. Humphreys: *Scripta Metall.*, 1974, vol. 8, p. 679.
29. A. Lasalmonie and J. L. Strudel: *Phil. Mag.*, 1975, vol. 32, p. 937.
30. A. J. Porter, R. A. Ricks, and R. C. Ecob: *J. Mat. Sci.*, 1983, vol. 18, p. 1895.
31. H. I. Aaronson: in *Decomposition of Austenite by Diffusional Processes*, V. F. Zackay and H. I. Aaronson, eds., Interscience Publishers, New York, NY, 1960, p. 387.
32. R. F. Decker: in *Steel Strengthening Mechanisms Symposium*, Climax Molybdenum Co., Greenwich, CT, 1969, p. 147.
33. R. G. Davies and T. L. Johnson: in *Ordered Alloys: Structural Applications and Physical Metallurgy*, B. H. Kear, C. T. Sims, N. S. Stoloff, and J. H. Westbrook, eds., Claitor's Publishing Division, Baton Rouge, LA, 1970, p. 447.
34. B. Bergman: *Scand. J. Metall.*, 1975, vol. 4, p. 97.
35. T. B. Gibbons and B. E. Hopkins: *Met. Sci. J.*, 1971, vol. 5, p. 233.
36. V. Biss and D. L. Sponseller: *Metall. Trans.*, 1973, vol. 4, p. 1953.
37. D. D. Pearson, B. H. Kear, and F. D. Lemkey: in *Creep and Fracture of Engineering Materials and Structures*, B. Wilshire and D. R. J. Owen, eds., Pineridge Press, Swansea, UK, 1981, p. 213.